

Journal of Materials Chemistry B

Accepted Manuscript



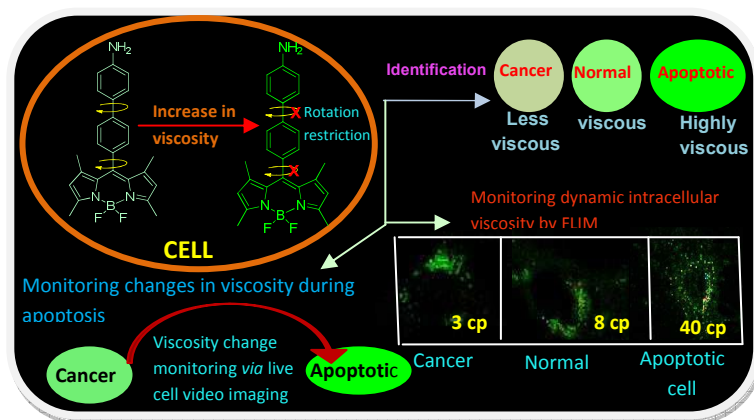
This is an *Accepted Manuscript*, which has been through the Royal Society of Chemistry peer review process and has been accepted for publication.

Accepted Manuscripts are published online shortly after acceptance, before technical editing, formatting and proof reading. Using this free service, authors can make their results available to the community, in citable form, before we publish the edited article. We will replace this *Accepted Manuscript* with the edited and formatted *Advance Article* as soon as it is available.

You can find more information about *Accepted Manuscripts* in the [Information for Authors](#).

Please note that technical editing may introduce minor changes to the text and/or graphics, which may alter content. The journal's standard [Terms & Conditions](#) and the [Ethical guidelines](#) still apply. In no event shall the Royal Society of Chemistry be held responsible for any errors or omissions in this *Accepted Manuscript* or any consequences arising from the use of any information it contains.

Graphical Abstract



The applications of a bodipy based probe **1** for identification of diseased cell population out of normal cells on the basis of changes in intracellular viscosity has been explored. The probe **1** works on the principle of restriction to rotation in viscous medium and the molecular rotor nature of probe **1** is supported by low temperature ^1H NMR and variable dihedral angle DFT and TD-DFT studies. More importantly, probe **1** is the first probe which shows its practical application to monitor micro-viscosity changes in cell based model system of undifferentiated, differentiated and apoptotic C6 glial cells. Further, probe **1** can effectively monitor apoptosis pathway by showing increase in fluorescence intensity from cancerous cell to apoptotic cell *via* real time live-cell video imaging. Moreover, the viscosity changes in living cells were proved by fluorescence lifetime imaging (FLIM) studies, flow cytometry using Annexin-V and Bcl-x1 expression by immunocytofluorescence (ICC) and western blot.



Journal Name

ARTICLE

A bodipy based fluorescent probe for evaluating and identifying cancer, normal and apoptotic C6 cells on the basis of changes in intracellular viscosity

Received 00th January 20xx,
Accepted 00th January 20xx

DOI: 10.1039/x0xx00000x

www.rsc.org/

Neha Gupta[†], Shahi Imam Reja[†], Vandana Bhalla[†], Muskan Gupta[†], Gurcharan Kaur[†] and Manoj Kumar^{†*}

The applications of a bodipy based probe **1** for identification of diseased cell population out of normal cells on the basis of changes in intracellular viscosity has been explored. The probe **1** works on the principle of restriction to rotation in viscous medium and the molecular rotor nature of probe **1** is supported by low temperature ¹H NMR and variable dihedral angle DFT and TD-DFT studies. More importantly, probe **1** is the first probe which shows its practical application to monitor micro-viscosity changes in cell based model system of undifferentiated, differentiated and apoptotic C6 glial cells. Further, probe **1** can effectively monitor apoptosis pathway by showing increase in fluorescence intensity from cancerous cell to apoptotic cell *via* real time live-cell video imaging. Moreover, the viscosity changes in living cells were proved by fluorescence lifetime imaging (FLIM) studies, flow cytometry using Annexin-V and Bcl-xl expression by immunocytofluorescence (ICC) and western blot.

Introduction

Cellular viscosity is a critical factor in governing diffusion-mediated cellular processes.¹ It strongly influences the interactions between biomolecules, intracellular transportation of mass and signal within live cells and consequently, the abnormal changes in cellular viscosity are related to many diseases and malfunction.² The increase in intracellular viscosity is associated with apoptosis while the decrease in intracellular viscosity predispose to cancer.³ Thus, monitoring of intracellular viscosity would be important to understand the pathological effects associated with abnormal viscosity levels in living systems. In literature, a number of molecular rotors have been reported for monitoring viscosity changes in cellular systems, sensing of proteins, nucleotides, enzymes, lipids etc.⁴ However, till date there is no report on utilization of molecular rotors for distinguishing between cancer, normal and apoptotic cells. Most of the reported molecular rotors are based on *meso*-substituted bodipy due to its good photo physical properties, non-toxic nature and easy cell permeability.⁵ However, these probes lack a perfect donor- π -conjugation-acceptor system which is the pre-requisite for a molecule to act as an efficient molecular rotor and thus cannot

detect ultra-low viscosity. Further, these probes have limited scope in the biological systems as these can only detect viscosity changes in dead cells, highly viscous membranes etc. (*vide supra*).^{5,6} Thus, monitoring of dynamic viscosity changes in living cells during pathological conditions like cancer, apoptosis etc has been handicapped by the lack of sensitive and efficient molecular rotors. Recently, Tang *et al.* reported AIE luminogen for detecting live and dead algae but the luminogen emits in blue region which sometimes interfere with auto-fluorescence of algal proteins. Moreover, the detection of intermediate stages between live and dead cells is not reported.⁷ From our laboratory, we reported a bodipy based molecule **3**^{5a} which shows turn off fluorescence response in the presence of H₂S leading to the formation of probe **1** having properties of molecular rotor (**Chart 1**).

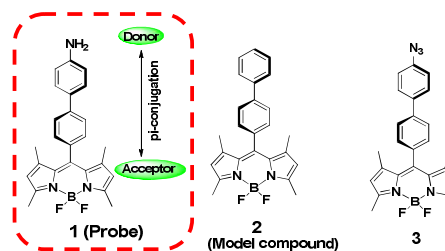


Chart 1: Structure of probe **1**, compound **2** and **3**

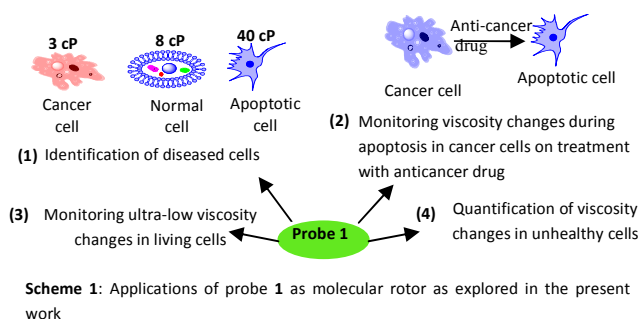
In continuation of this work, we were then interested to explore the applications of probe **1** as a molecular rotor for monitoring dynamic intracellular viscosity changes during pathological conditions and for identifying diseased cell population on the basis of viscosity (**Scheme 1**). We envisaged

[†] Department of Chemistry, UGC Sponsored Centre for Advanced Studies-1, Guru Nanak Dev University, Amritsar, Punjab, India.

E-mail: mksharmaq@yahoo.co.in

[‡] Department of Biotechnology, Guru Nanak Dev University, Amritsar, Punjab, India.

Electronic Supplementary Information (ESI) available: [details of any supplementary information available should be included here]. See DOI: 10.1039/x0xx00000x



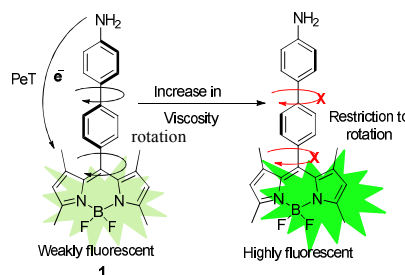
that incorporation of two phenyl rings (rotating units) at *meso*-position will cause maximum deactivation of excited state through non-radiative pathway which will make rotor more sensitive to environment and further introduction of an amino group at the phenyl ring will make the molecular rotor more sensitive to low viscosity because it makes a perfect donor- π -conjugation-acceptor (D- π -A) system. To the best of our knowledge, this is the first report where a molecular rotor has been used for identifying diseased cells on the basis of changes in viscosity. Moreover, probe **1** has many advantages: (i) Probe **1** acts as an efficient sensing tool for monitoring viscosity changes in cell based model system consisting of undifferentiated cancer cells, differentiated normal cells and apoptotic C6 glial cells. (ii) It is further used for quantitative mapping of dynamic intra-cellular viscosity of different cells *via* fluorescence lifetime imaging (FLIM) studies. (iii) More significantly, probe **1** is further utilized to monitor viscosity changes during apoptosis caused by camptothecin in C6 glial cells *via* live-cell video imaging.

Results and discussion

Probe **1** was synthesized by the reported method (ESI[†] Scheme S1).^{5a} The fluorescence spectrum of probe **1** in methanol exhibits a weak emission at 517 nm when excited at 470 nm. This is mainly due to free rotation of *meso*-substituted phenyl rings and slightly due to photo induced electron transfer (PeT) from the lone pair of electrons on nitrogen to photo-excited bodipy moiety (**Scheme 2**).⁸ However, on increasing the viscosity from 0.6 to 950 cP (methanol: glycerol, 0-99%), the fluorescence of probe **1** increases at 517 nm.^{5a} The fluorescence lifetime of probe **1** also increases from 2.34 ns to 4.35 ns with the gradual increase in viscosity which indicates the restriction to rotation of phenyl rings when excited at 488 nm (see ESI[†] table S1). We also carried out fluorescence life time studies of probe **1** in methanol-glycerol mixture (1:1, v/v) at variable temperature (0 to 80 °C). It was observed that the decay time of probe **1** is higher (3.42 ns) at 0°C and lower (2.23 ns) at 80 °C (ESI[†] Fig. S4). This is probably due to the fact that increase in temperature changes the viscosity of glycerol. Further, to confirm that whether temperature or viscosity is affecting the fluorescence lifetime of probe **1**, we studied the fluorescence lifetime of probe **1** in varying methanol: glycerol mixture (0, 50, 70, and 100% glycerol) at temperatures between 293 K to 333 K and the data is compiled in one graph (ESI[†] Fig. S5). From the graph, it is clear that in methanol

alone, probe **1** does not show significant change in decay time with increase in temperature which is probably due to the fact that the viscosity of methanol is less affected by temperature. However, in methanol: glycerol mixture (with high glycerol concentration, 70, 90 and 100% glycerol), the decay time varies with temperature because the viscosity of glycerol decreases with increase in temperature. From these studies, we may conclude that temperature does not directly alter the lifetime of probe **1** except changing the viscosity of the medium.^{4k}

Further, we utilized Fröster–Hoffmann equation⁹ to correlate the relationship between emission intensity of probe **1** and the



Scheme 2: Working principle of the probe **1**

solvent viscosity (Equation 1).

$$\log I = C + x \log \eta \quad (1)$$

where η is the viscosity, I is the emission intensity, C is a constant and x corresponds to the sensitivity of the probe to viscosity. The probe shows linear relationship between $\log I$ and $\log \eta$ ($R^2 = 0.9914$). Interestingly, the value of x is as high as 0.52 (ESI[†] Fig. S6)

Further, to justify that probe **1** with amino group acts as an effective molecular rotor, we synthesized a model compound **2** (**Chart 1**). The structure of compound **2** was characterized from its spectroscopic data (ESI[†] scheme S1 and fig S1-S3). The fluorescence spectrum of compound **2** in methanol exhibits an emission band at 510 nm when excited at 470 nm. The initial fluorescence intensity of compound **2** in methanol is higher than the fluorescence intensity of probe **1** in methanol which indicates the absence of PeT in compound **2**. On addition of glycerol, the fluorescence intensity of compound **2** increases but the increase is only 4.2 folds (ESI[†] Fig. S7). Further, we studied the fluorescence lifetime behavior of compound **2** in different methanol-glycerol fractions and it was found that at 0% glycerol the decay time is higher than the decay time of probe **1** and with increasing viscosity, it increases from 2.47 ns to 3.89 ns (ESI[†] Fig. S8) which is less compared to probe **1** (from 2.34 ns to 4.35 ns). These studies indicate the role of amino group (PeT donor) in making probe **1** as an efficient molecular rotor by providing efficient D- π -A system because in viscous medium; when rotation gets restricted, PeT also becomes unfavourable leading to increase in fluorescence emission. To further support the molecular rotor nature of probe **1**, we carried out variable temperature ¹H NMR studies. It was observed that a singlet for the methyl protons at 1 and 7 positions of bodipy core appears at 1.40 ppm when the ¹H NMR spectrum was recorded at 25°C. However, an up-field

shift of 0.04 ppm in the methyl protons was observed at -25°C (ESI† Fig. S9 and S10). This up-field shift is due to the shielding effect generated by the restriction of rotation of phenyl rings (orthogonal conformation).^{5c}

Further, we studied the effect of solvent polarity on the fluorescence behaviour of probe **1** (table 1). It was found that probe **1** is weakly emissive in polar solvents compared to non-polar solvents (ESI† Fig. S11).

Solvent	Dielectric constant	η (cP)	λ_{abs} (nm)	λ_{em} (nm)	ϵ ($\text{M}^{-1}\text{cm}^{-1}$)	Quantum yields (Φ)	Average decay time (τ_{avg}) (ns)
Benzene	2.27	0.60	493	512	68400	0.18	2.29
Toluene	2.38	0.56	494	513	69700	0.17	2.30
THF	7.6	0.53	497	516	63200	0.12	2.34
ACN	37.5	0.37	498	515	61200	0.08	2.26
DCM	9.1	0.43	498	516	60600	0.07	2.24
Dioxane	2.2	1.54	500	515	73800	0.11	2.02
EtOH	24.3	1.20	500	517	85000	0.13	2.19
MeOH	32.4	0.60	499	517	72600	0.10	2.34
DMSO	48.9	2.24	500	518	75000	0.14	2.63
H ₂ O	78.4	1.01	500	517	62200	0.03	2.25
Glycerol	45.8	950.17	501	518	91400	0.82	4.35

Table 1: Compiled photo-physical data of the probe **1** in different solvent system.

This is due to the fact that PeT is more favourable in polar solvents.¹⁰ However, in glycerol maximum fluorescence emission enhancement and higher lifetime was observed due to restriction to rotation and also by decrease in solvent relaxation¹¹ which thereby makes the PeT process unfavourable (ESI† Fig. S11 and S12). From these studies, it is clear that solvent polarity has relatively less effect on fluorescence emission of probe **1** in comparison to increase in viscosity. We also calculated the rate constants for the radiative (k_r) and non-radiative (k_{nr}) pathways using the following equations:

$$k_r = \Phi/\tau_{\text{avg}} \quad (2)$$

$$k_{nr} = (1-\Phi)/\tau_{\text{avg}} \quad (3)$$

With increase in viscosity from 0.6 cP to 950 cP, the rate constant for the radiative (k_r) (Equation 2) pathways increases

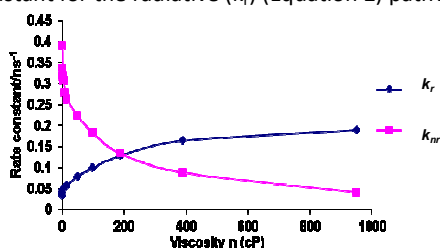


Fig. 1: The radiative (k_r) and non-radiative (k_{nr}) rate constants for probe **1** recorded in methanol-glycerol mixtures of various compositions, plotted against the viscosity of mixtures.

from $0.03846 \times 10^9 \text{ s}^{-1}$ to $0.18850 \times 10^9 \text{ s}^{-1}$, whereas the rate constant for non-radiative (k_{nr}) pathways (Equation 3) decreases from $0.38889 \times 10^9 \text{ s}^{-1}$ to $0.04137 \times 10^9 \text{ s}^{-1}$ i.e., non-

radiative processes were gradually suppressed (Fig. 1 and Table 2).¹² However, the increase in k_r is only 3.9 folds while the decrease in k_{nr} is 8.4 folds, indicating that for molecular rotors k_{nr} mainly changes with increase in viscosity. The plot of k_r and k_{nr} with respect to increasing viscosity indicates that the decrease in k_{nr} is higher in comparison to increase in k_r (Fig. 1).

Glycerol: Methanol (V/V) at 25 °C	Average decay time (τ_{avg})	Quantum yield (Φ)	Rate constant for radiative pathways (k_r) (s^{-1})	Rate constant for non-radiative pathways (k_{nr}) (s^{-1})
0:10	2.34 ns	0.09	0.03846×10^9	0.38889×10^9
1:9	2.65 ns	0.11	0.04150×10^9	0.33584×10^9
2:8	2.74 ns	0.13	0.04744×10^9	0.31751×10^9
3:7	2.81 ns	0.14	0.04982×10^9	0.30604×10^9
4:6	3.02 ns	0.16	0.05298×10^9	0.27814×10^9
5:5	3.12 ns	0.18	0.05769×10^9	0.26282×10^9
6:4	3.31 ns	0.26	0.07854×10^9	0.22356×10^9
7:3	3.54 ns	0.35	0.09887×10^9	0.18361×10^9
8:2	3.82 ns	0.49	0.12827×10^9	0.13350×10^9
9:1	3.96 ns	0.65	0.16414×10^9	0.08838×10^9
10:0	4.35 ns	0.82	0.18850×10^9	0.04137×10^9

Table 2: Compiled data of the rate constant of radiative and non-radiative pathways of probe **1** with varying glycerol: methanol fraction.

The increase in k_r is due to the fact that two pyrrole rings of bodipy framework attain planarity in highly viscous medium. Thus, probe **1** exhibits sensitivity towards viscosity of the environment. Further, we studied the effect of pH on the fluorescence behaviour of probe **1**. There was a negligible fluorescence enhancement on lowering the pH from 7.4 to 4 (ESI† Fig. S13). On further lowering the pH from 4 to pH 2, there was slight enhancement in fluorescence intensity of probe **1** (0.91 folds) which is probably due to suppression of PeT. To find out the reason why there was a negligible fluorescence enhancement on lowering the pH from 7.4 to 4, we calculated the pKa value of probe **1** which was found to be 3.9 (ESI† Fig. S14). From this pKa value and pH studies, it is clear that probe **1** is not sensitive to the pH of the environment. Thus, we may conclude that probe **1** will show no interference of intracellular pH as it will not be less than pH 4. Further, to study the selectivity of probe **1** towards viscosity, we carried out the fluorescence studies of probe **1** in the presence of other potentially competing species such as Cys, Hcy, GSH, ClO^- , H_2O_2 , HS^- , ascorbic acid etc. However, the addition of these analytes did not induce any observable change in fluorescence emission intensity at $\lambda_{\text{em}} = 517 \text{ nm}$ which indicates that the probe **1** is selective for viscosity (ESI† Fig. S15). We also carried out DFT and TD-DFT calculations using B3LYP/6-31G(d,p) level of Gaussian 09¹³ to prove the molecular rotor nature of probe **1**. The DFT calculations in gas phase have shown that both the HOMO and LUMO of probe **1** are localized on the BODIPY moiety, which indicates that probe **1** is a typical donor-acceptor (D–A) system with no charge transfer in the ground state in gas phase (ESI† Fig. S16). However, when we consider the effect of solvent, then, the results provide a more complicated picture than in gas phase. In methanol, the HOMO is now centered on the aminophenyl

moiety and the MO centered on the bodipy is the next lowest one (HOMO-1). Further, we investigated the effect of different

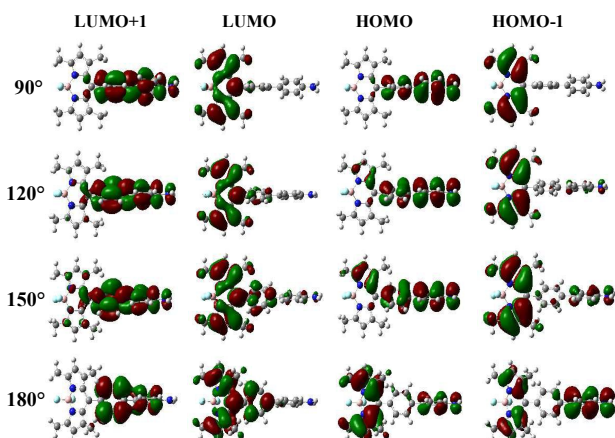
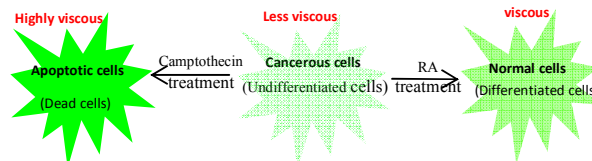


Fig. 2: The molecular orbitals of probe **1** with respect to the optimized geometries of probe **1** in the excited states at different dihedral angles around C36-C21-C10-C11

solvents (polar and non-polar) on the fluorescence behaviour of probe **1** in order to justify the PeT phenomenon. It was observed that in polar solvents the electron density of the HOMO is localized on the aminophenyl moiety while LUMO is localized on the bodipy core. This distribution of electron density on the HOMO and LUMO of probe **1** in polar solvent represents a perfect picture of charge separation which is favourable for PeT phenomenon.¹⁴ However, in case of non-polar solvents like benzene and toluene; both HOMO and LUMO are localized on the bodipy core which indicates that there is no charge separation in this case and hence PeT is less effective (ESI[†] Fig. S17 and S18). We then carried out scan of the dihedral angle between the bodipy core and phenyl ring (C36-C21-C10-C11) and ran TD-DFT scan at 30° of rotational barrier. In a situation, when the dihedral angle is 90° i.e., the orthogonal conformation, the HOMO is centered on the aminophenyl moiety and LUMO is oriented on bodipy core. This orbitals picture indicates that there is chance for electron transfer from aminophenyl moiety to bodipy core. However, in higher viscosity, probe **1** attains planarity^{5b} i.e., planar conformation (dihedral angle is 180°). In the planar conformation (bodipy ring is slightly distorted), the HOMO no longer exists at aminophenyl moiety and the drift of electron cloud occurs from aminophenyl moiety to bodipy core (**Fig. 2** and ESI[†] Fig. S19). Hence, there is no chance for the PeT phenomena in this situation. To further justify the rotation phenomena in probe **1**, we carried out the scan of probe **1** at different dihedral angles in S_0 and S_1 states of probe **1**. Smaller the energy difference between S_0 and S_1 states, easier will be the non-radiative decay.¹⁵ From the scan results, it was observed that the energy gap between the S_0 and S_1 states is lower in orthogonal conformations and maximum in coplanar conformation which indicates that for orthogonal conformation, maximum non radiative decay phenomena was observed and minimum for the coplanar conformation (ESI[†] Fig. S20 and S21). Further, we also carried out similar scan

studies for compound **2** and it was observed that compound **2** also displays similar results but the effect is far less in comparison to probe **1** (ESI[†] Fig. S22). To compare the scan results of probe **1** and compound **2**, the energy gaps of probe **1** and compound **2** are combined together in one graph. From the graph, it is clear that probe **1** act as a better molecular rotor than the model compound **2** (ESI[†] Fig. S23).

Having done all this, we were then interested to study the biological applications of probe **1** for monitoring intracellular viscosity changes in living cells during pathological conditions. Before carrying out the cell imaging of probe **1**, we performed the MTT assay studies to check the cytotoxicity of probe **1**.¹⁶



Scheme 3: Schematic representation of cell based model system of C6 glial cells.

The cytotoxicity of the probe **1** was very low during 24 h of incubation period. The MTT assay showed that >95% of C6 cells survived after 12 h, and after 24 h, the cell viability remained at ~90% which indicates that probe **1** can be safely used for biological studies (ESI[†] Fig. S24). Since, we were interested to monitor the viscosity changes in healthy and diseased cells, we used the cell based model systems of cancer (undifferentiated cells), normal (differentiated cells) and apoptotic C6 glial cells (**Scheme 3**). We envisaged that the fluorescence intensity of probe **1** will increase with restriction to rotation resulting from increased intracellular viscosity, as cells undergoes various physiological changes, cancerous to normal differentiated and apoptotic state (**Scheme 3**). In general, cancer cells are less viscous due to their rapidly dividing nature and apoptosis resistance property¹⁷ while normal cells are viscous than cancer cells as they have the property to undergo apoptosis.¹⁸ First, we incubated cancer cells (undifferentiated cells) with probe **1** for 30 min and then cell imaging was performed. Cell imaging results showed weak fluorescence intensity of probe **1** in undifferentiated C6 glioma cells (**Fig. 3A**). Further, cancer (undifferentiated) cells were treated with retinoic acid (RA) which is known to induce differentiation i.e., conversion of undifferentiated cells to normal phenotype.¹⁹ The RA treated cells were then incubated with probe **1** and cell imaging was performed which showed higher fluorescence intensity (**Fig. 3B**). However, to verify that the fluorescence enhancement on moving from cancer to normal cell is due to increased viscosity and not due to retinoic acid, we carried out the fluorescence titration of probe **1** with retinoic acid (ESI[†] Fig. S25). No fluorescence enhancement was observed which indicates that the increase in fluorescence intensity is due to increase in intracellular viscosity. Generally, the undifferentiated cancerous cells do not undergo apoptosis, so, to induce apoptosis in cancer cells we treated cancer cells with an apoptosis inducer drug camptothecin which intercalates into the Topoisomerase (TOPO1)-DNA complex

(cleavable complex).²⁰ Cells were then incubated with probe **1** and cell imaging was performed. Apoptotic cells showed highest fluorescence intensity (Fig. 3C). The highest fluorescence intensity in apoptotic cells is due to high viscosity

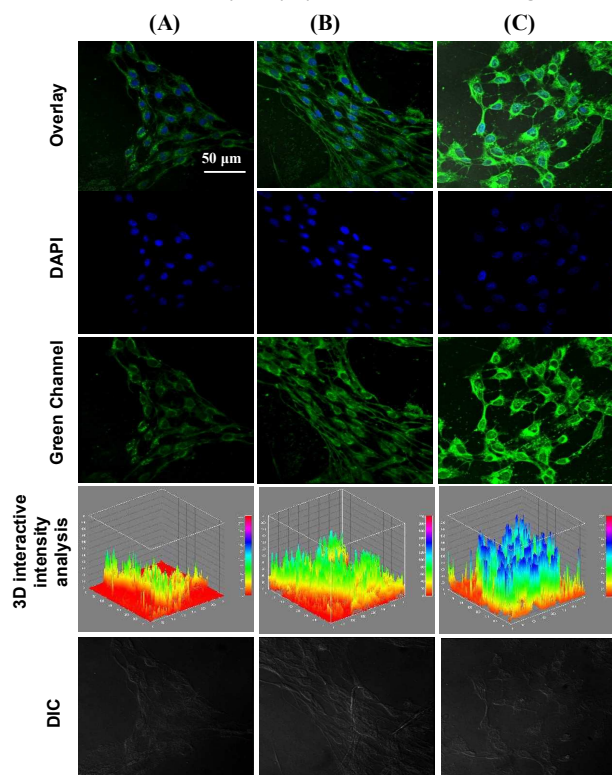


Fig. 3: Confocal images of the probe **1** expression in C6 glioma cells. (A) Undifferentiated C6 glioma cells exposed to probe **1** (5.0 μM) for 30 min. (B) RA differentiated C6 glioma cells group. Undifferentiated C6 glioma cells first treated with 10.0 μM RA, a potent differentiation inducer, after every 24 hours for 4 days, then exposed to the probe **1** for 30 min. (C) Apoptotic cells group. Undifferentiated C6 glioma cells were treated with 100 μM Camptothecin, a known apoptosis inducer drug and then exposed to 5.0 μM of probe **1** for 24 hours. scale bar 50 μm.

in these cells and this is in good agreement with the proposed hypothesis of cell based model systems showing maximum intensity for apoptotic cells, and relatively lower for differentiated cells and minimum for undifferentiated cells. The above results provide a clear justification for the proposed hypothesis and simultaneously prove that probe **1** acts as a marker for sensing viscosity changes in different types of cells. Further, to quantify the intensity enhancement in these different cell models, we performed intensity analysis and calculated the relative fluorescence intensity of undifferentiated cancer, differentiated normal and apoptotic C6 glioma cells which was found to be 100, 120 and 200 au (ESI† Fig. S26). Moreover, the 3D interactive intensity plots of cell based model system clearly represents the viscosity changes in different cells as represented in fig. 3.

Generally, the intracellular viscosity changes were observed to be associated with apoptosis phenomenon. Thus, to confirm the role of apoptosis for viscosity changes in cell based model system of C6 glioma cells; we carried out studies using apoptosis marker,²¹ immunocytofluorescence (ICC) and western blot for

the expression of Bcl-xl (anti-apoptotic marker) in cancer and RA treated C6 glioma cells.²² The flow cytometer results of cell based model system show that cancer cells have less number of early and late apoptotic cell population while RA and camptothecin treated C6 cells had higher number of early and late apoptotic cells (Fig. 4A and ESI† Fig. S27). These results prove that cancer cells do not undergo apoptosis easily and thus are less viscous while RA and camptothecin treated cells had higher rate of apoptosis and due to this reason these were

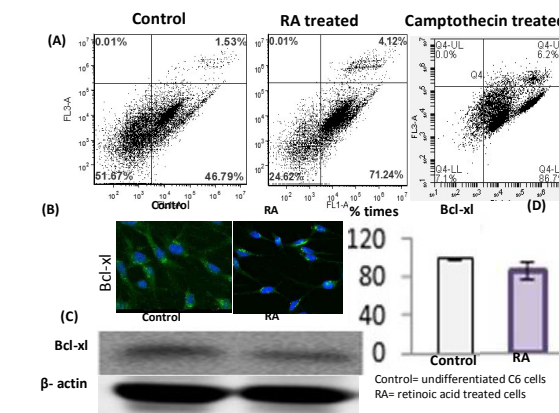


Fig. 4: (A) Flow cytometer analysis of cell based model of C6 cells. (B) Immunocytofluorescence studies showing reduced expression of Bcl-xl in RA treated cells (C) Western blot (D) Plot comparing Bcl-xl expression in control and RA treated cells.

more viscous than cancer cells. Further, we studied the expression of Bcl-xl, an anti-apoptotic marker in cell based model system. This Bcl-xl is expressed in non-apoptotic cells and when apoptosis is initiated in cells, its expression starts suppressing.²³ The expression of Bcl-xl significantly decreased in RA treated cells in comparison to cancer undifferentiated cells as assessed by immunocytofluorescence (Fig. 4B and ESI† Fig. S27). Moreover, western blotting result also confirms a significant down regulation of Bcl-xl expression as cells move from cancer to normal phenotype (Fig. 4C,D). This data explains the underlying mechanism for the enhancement in fluorescence intensity due to increase in viscosity of C6 glioma cells as we move from cancer to normal and apoptotic cells. We further explored the efficacy of the probe **1** to monitor intracellular viscosity changes by choosing two different cell lines. We chose C6 cell line (as cancer cell model) and BV2 cell line (as normal cell model) for monitoring intracellular viscosity changes by probe **1**. Both C6 and BV2 cell lines were incubated with same concentration of probe **1** (5.0 μM) for 30 min and then cell imaging was performed. The cell imaging results show that BV2 cells had higher fluorescence intensity than the C6 cells (ESI† Fig. S28), which further confirms the sensitivity of probe **1** towards intracellular viscosity changes. Thus, probe **1** has the potential to distinguish cancer cells from normal cells. Since viscosity increases gradually during the apoptosis, so, we further monitored the real-time viscosity changes during apoptosis in C6 undifferentiated cells with addition of camptothecin. C6 cells were first internalized with probe **1** (5.0 μM) and washed with PBS buffer and then camptothecin (100 μM) was added. Fluorescence images were recorded at

different time intervals of 0, 30, 60, 90, 120, 150, 180, 210, 240, and 300 min *via* live-cell video imaging (Fig. 5 and zip file). Camptothecin induces apoptosis in the undifferentiated cells with time and the changes in viscosity during apoptosis are demonstrated in a time dependent manner in images. Moreover, the control experiment (without Camptothecin) showed no significant change in fluorescence intensity of probe **1** with time (ESI† Fig. S29). The increase in fluorescence

intensity of probe **1** with time on treatment with camptothecin is attributed to the fact that cells are undergoing apoptosis which leads to increase in intracellular viscosity. These viscosity changes are well represented in 3D interactive intensity analysis plots in Fig 5B. Thus, the above results clearly indicate that the probe **1** can be used for monitoring viscosity changes during apoptosis pathways in living system.

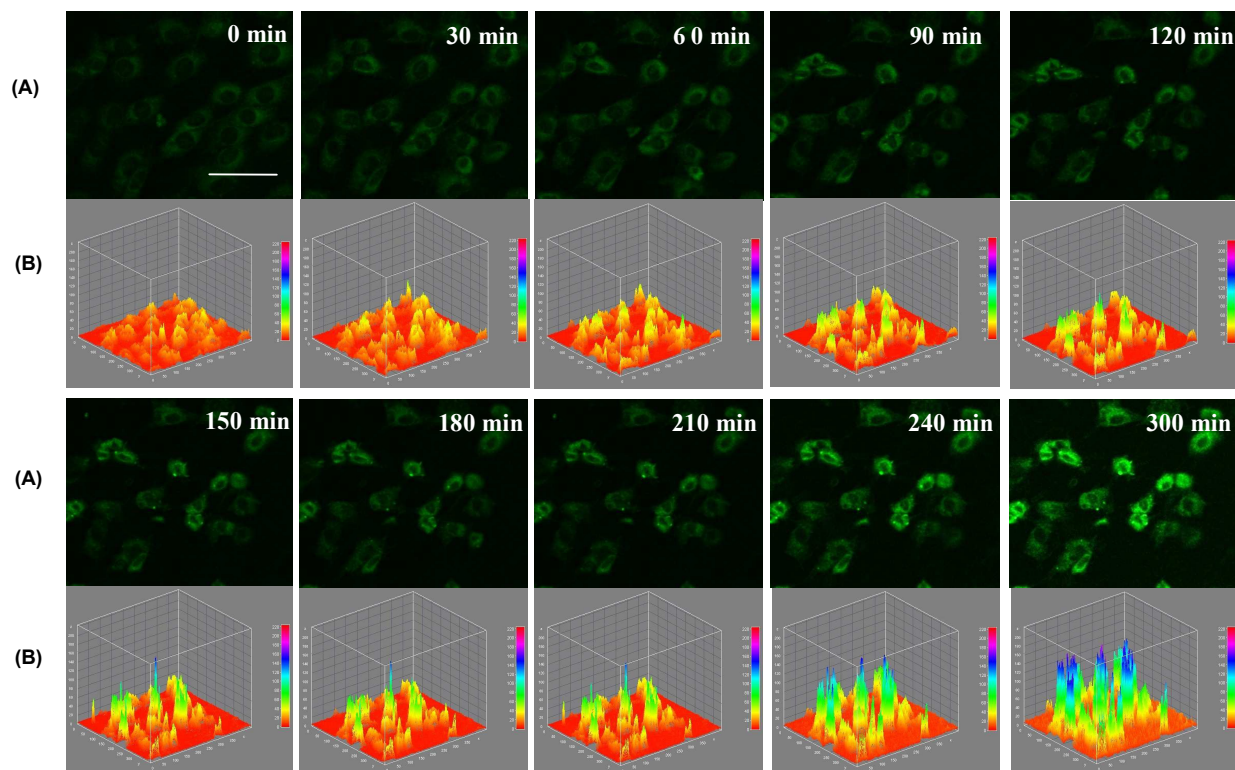


Fig. 5: (A) Fluorescence images of C6 glioma cells (B) 3D interactive intensity analysis of probe **1** (5.0 μM) at different time points after addition of camptothecin (100 μM). Images are acquired by using excitation and emission windows of $\lambda_{\text{ex}} = 488$ and $\lambda_{\text{em}} = 500\text{--}550$ nm, respectively; Scale bars: 50 μm .

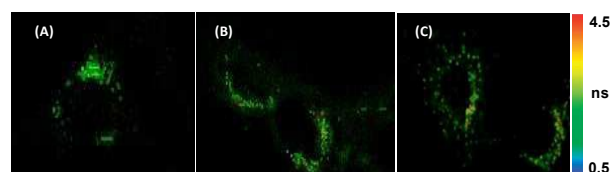


Fig. 6: (A) FLIM of C6 cells treated only probe **1** (5.0 μM); (B) C6 cells treated with RA and then incubated with probe **1**; (C) C6 cells treated with camptothecin and then incubated with probe **1**. Emission was detected at 500–530 nm using an inverted-type laser scanning confocal microscope.

Further, for quantitative viscosity mapping in living cells, we carried out fluorescence lifetime imaging (FLIM)^{4a,f} with high spatial resolution in C6 glial cell lines using probe **1** (Fig. 6). The FLIM studies showed that the local micro-viscosity of the cells increases on moving from cancerous to normal to apoptotic cells. According to life time histogram, the life time of probe **1** in cancer, normal and apoptotic C6 cells are 2.8 to 3.02 and to 3.26 ns respectively which indicates that

apoptotic cells have high viscosity compared to normal and cancer cell (ESI† Fig. S30 and Table S2). Moreover, the cancer cells showed the least micro-viscosity which is in good agreement with the above fluorescence intensity analysis. Further, from the calibration curve, the viscosity in cancer, normal and apoptotic cells was found to be 2.5 ± 0.5 , 8 ± 1 and 40 ± 2 cP²⁴ (ESI† Fig. S31). Thus, probe **1** in combination with the FLIM studies acts as an efficient platform for monitoring dynamic intracellular viscosity of different cells.

Conclusions

In conclusion, a bodipy based molecular rotor probe **1** has been utilized to distinguish cancer, normal and apoptotic cells on the basis of intracellular viscosity changes in living cells. The practical applicability of probe **1** as biosensor for identifying diseased cell population out of normal cell population is described using cell based model system of C6 glial cells. The viscosity changes associated with apoptosis were proved by apoptosis marker studies using Annexin-V

and Bcl-Xl. Moreover, the strategy of monitoring viscosity changes in cells by converting cancer cells to normal and apoptotic is unprecedented and helps to identify disorders and diseases in living system. More importantly, probe **1** is practically applied in real-time quantification of intracellular viscosity changes during apoptosis pathway in live cells. It is therefore, believed that probe **1** along with FLIM studies provides a promising strategy in the design of probes for sensing viscosity and monitoring the apoptosis pathways. Hence, probe **1** reported herein is an efficient tool for diagnosis of viscosity related diseases and will attract more attention to discover more sensors to investigate cellular viscosity related to diseases and pathology.

Experimental

Materials and instrumentation

The reagents were purchased from Aldrich and used without further purification. For the photo-physical studies, HPLC grade solvents (CH₃CN, DMSO, DMF, Dioxane, EtOH, MeOH, THF, DCM) were used. SHIMADZU UV-2450 spectrophotometer was used for recording UV-vis spectra having a quartz cuvette (path length 1 cm). The cell holder was thermostatted at 25 °C. The fluorescence spectra were recorded using SHIMADZU 5301 PC spectrofluorimeter. Bruker AVANCE III HD 500 MHz spectrophotometer was used for recording ¹H NMR spectra using CDCl₃ as solvent and tetramethylsilane as the internal standard. Data are reported as follows: chemical shift in ppm (d), multiplicity (s = singlet, d = doublet, t = triplet, m = multiplet, br = broad singlet), coupling constants *J* (Hz).

Synthesis of compound 2:

To a solution of 4-bromo bodipy **4** (0.100 g, 0.2480 mmol) and phenyl boronic acid (0.037 g, 0.30 mmol) in dioxane (20 mL) were added K₂CO₃ (0.137 g, 0.992 mmol), distilled water (1 mL), and Pd(0) (0.063 g, 0.054 mmol) under nitrogen, and the reaction mixture was refluxed overnight. The dioxane was then removed under vacuum, and the residue so obtained was treated with water, extracted with dichloromethane, and dried over anhydrous Na₂SO₄. The organic layer was evaporated, and the compound was purified by column chromatography using hexane/chloroform (8:2, v/v) as an eluent to give 0.089 g (57 %) of compound **2** as orange coloured solid. ¹H NMR (CDCl₃, 500 MHz, ppm) 1.47 (s, 6 H), 2.59 (s, 6 H), 6.02 (s, 2 H), 7.38 (d, *J* = 5 Hz, 2 H), 7.42 (t, *J* = 5 Hz, 1 H), 7.51 (t, *J* = 5, 2 H), 7.71 (d, *J* = 5, 2 H), 7.78 (d, *J* = 5, 2 H). ¹³C NMR (CDCl₃, 100 MHz, δ = ppm) = 14.55, 14.60, 29.79, 50.90, 121.25, 127.64, 127.87, 128.50, 128.96, 131.48, 133.94, 139.99, 141.72, 143.15, 155.51. ESI-MS *m/z* 400.4393 (M)⁺.

UV-vis and Fluorescence studies

The solutions of probe **1** and compound **2** of different viscosities were prepared by adding the stock solution of probe **1** and compound **2** to the solvent mixture (3 mL; methanol/glycerol) with varying fractions of methanol and

glycerol to obtain the final concentration of the dye (5.0 μM). These solutions were sonicated for 5 min to eliminate air bubbles. After standing for 1 h at a constant temperature, the solutions were used for UV-vis and fluorescence studies. Fluorescence quantum yields were determined by using optically matching solution of fluorescein (Φ_{fr} = 0.95 in 0.1M NaOH solution) as standard at an excitation wavelength of 470 nm and quantum yield is calculated using the equation:

$$\Phi_{is} = \Phi_{fr} \times \frac{1-10^{-A_r L_r}}{1-10^{-A_s L_s}} \times \frac{N_s^2}{N_r^2} \times \frac{D_s}{D_r}$$

Φ_{is} and Φ_{fr} are the radiative quantum yields of sample and the reference respectively, A_s and A_r are the absorbance of the sample and the reference respectively, D_s and D_r are the respective areas of emission for sample and reference. L_s and L_r are the lengths of the absorption cells of sample and reference respectively. N_s and N_r are the refractive indices of the sample and reference solutions.

Procedure for theoretical calculations (DFT and TD-DFT studies)

All the theoretical calculations were done using Gaussian 09 software. The geometry of probe **1** and compound **2** was optimized using density functional theory (DFT) and time-dependent density functional theory (TD-DFT) with the Becke three-parameter hybrid exchange function with the Lee–Yang–Parr gradient-corrected correlation functional (B3-LYP functional) and in B3LYP/6-31G(d,p) basis set. All the atoms were free to optimize and no constraints to bonds/angles/dihedral angles were applied in the calculations. The potential energy curves for the S₀ state were qualitatively scanned by constrained optimizations, with the dihedral angles kept at fixed values. The potential-energy curves for the S₁ state were obtained by calculating the Frank–Condon transition energies for the ground-state optimized structures at fixed dihedral angles by using the time-dependent (TD)-DFT method. Integral equation formalism polarizable continuum model (IEFPCM) with different solvent system was used for solvent dependent studies.

Fluorescence lifetime studies

The fluorescence lifetime spectra were recorded using HORIBA time-resolved fluorescence spectrometer and lifetimes were obtained by time-correlated single photon-counting (TCSPC) device. The fluorescence lifetime of probe **1** and compound **2** was measured with an excitation wavelength at λ_{ex} = 488 nm and emission at λ_{em} = 517 and 510 nm. All decay experiments were carried out in a 3 mL quartz cuvette having 5 μM of probe concentration. In-built software allowed the fitting of the decay spectra (χ² ≈ 1) and yielded the fluorescence lifetimes. Decay curves were fitted as a single exponential. The equation is:

$$I(t) = \sum_{i=1}^M A_i \exp(-t/\tau_i)$$

In our case $\tau(t) = \tau_0 = \text{constant}$, which leads to classical single-exponential decay function and the above equation reduced to:

$$I(t) = A_0 \exp(-t/\tau_0)$$

where τ_0 is the emission lifetime and A_0 is the amplitude of the pre-exponential.²⁵

Cell based model studies

C6 Cells were maintained in DMEM supplemented with 1X PSN (GIBCO), 10% FBS (Biological Industries) at 37°C and humid environment containing 5% CO₂. For fluorescence detection, cells were seeded on 18 mm coverslips in 24 well plates. For monitoring viscosity changes in different types of cells, we planned cell based model studies. In the cell model system, three groups were considered: **I.** Undifferentiated cancerous C6 glioma cells: Cells were treated with probe **1** (5.0 μM) with an incubation period of 30 min. **II.** Differentiated cells, for which undifferentiated C6 glioma cells were treated with 10 μM RA after every 24 h for 4 days to induce differentiation of glioma cells. RA converts cancer cells to normal phenotype. Then, cells were exposed to the 5.0 μM probe **1** for 30 min. and **III.** Apoptotic cells, for which undifferentiated C6 glioma cells were treated with 100 μM Camptothecin followed by 5.0 μM of probe **1** exposure for 24 hours. After treatment, cells were washed three times with 2 mL PBS at room temperature, and then observed under a confocal microscopy.

Fluorescence imaging

C6 and BV2 cells were supplemented were seeded in 24-well and 12-well plates and then incubated for 24 hrs at 37°C temperature under 5% CO₂. Both C6 and BV2 cells were incubated with probe **1** (5.0 μM) for 30 min. After treatment both types of cells were washed three times with PBS at room temperature, and then observed under a confocal microscopy and images were captured using excitation wavelength of $\lambda_{\text{ex}} = 488 \text{ nm}$.

Fluorescence lifetime imaging (FLIM)

The fluorescence lifetime imaging (FLIM) studies were carried out with an inverted-type laser scanning confocal microscope with a 60X objective. The emission was collected through a 500 ± 30 nm band pass filter. For imaging studies, C6 cells were supplemented with 10% fetal bovine serum. The cells were seeded in 24-well flat-bottomed plates and then incubated for 24 hrs at 37 °C under 5% CO₂. Probe **1** (5.0 μM) was then added to the C6 cells and incubated for another 30 min. The cells were washed three times with 2 mL PBS at room temperature, and then observed under a confocal microscopy. For cell apoptosis studies, C6 cells were incubated with camptothecin and then exposed to probe **1** (5.0 μM) for 24 hrs.

Procedure of Western blotting

For total protein extraction, C6 glioma cells were grown and treated in 100 mm petri dishes followed by harvesting with PBS-EDTA (1 mM). The cell pellet was homogenized in RIPA buffer (50 mM Tris; pH 7.5), 150 mM NaCl, 0.5 % sodium deoxycholate, 0.1% SDS, 1.0% NP-40) and protein concentration was determined by the Bradford method. Protein lysate (30 μg) was resolved in 10% gel by Sodium dodecyl sulphate-Polyacrylamide gel electrophoresis (SDS-PAGE), followed by transfer onto a PVDF membrane (Hybond-P) using the semi-dry Novablot system (Amersham Pharmacia). Further, membranes were probed with mouse monoclonal anti-Bcl-xl (1:1,000) for overnight at 4 °C. This was followed by washing with 0.1 % TBST and incubation with HRP labelled secondary antibodies for 2 h at RT. Immunoreactive bands were detected by ECL Plus Western blot detection system (Amersham Biosciences) using LAS 4000 (GE Biosciences). Actin has been used as an endogenous control for normalizing the expression of the protein of interest. The change in expression of gene of interests was the average of IDV values obtained from at least three independent experiments.

Procedure of Flow cytometry (Annexin-V-FITC study for apoptosis)

To confirm apoptotic and necrotic cell death by camptothecin and not by retinoic acid, cells were stained with annexin V conjugated with FITC and PI using the annexin V-FITC apoptosis Detection Kit (Miltenyi Biotech), according to the manufacturer's protocol. Annexin V has a high affinity for phosphatidylserine exposed on the outer membrane of apoptotic cells, while PI is transported to late-stage apoptotic/necrotic cells with disrupted cell membranes. The cells from control and treated groups were trypsinized, washed with PBS, and resuspended in 1ml of Annexin V binding buffer (1X) with addition of 10 μl Annexin VFITC. Following incubation (for 15 min in the dark at room temperature) and centrifugation (5 min, 300xg), 500 μl of Annexin V binding buffer and 5 μl of PI were added to the cell pellet and incubated for further 5 min in the same conditions. Viable (Annexin V-, PI-negative), early apoptotic (Annexin V-positive, PI-negative), late apoptotic (Annexin V-, PI-positive) and necrotic (Annexin V-negative, PI-positive) cells were detected by flow cytometry (Accuri C6 flow cytometer; Becton-Dickinson) and quantified by BD Accuri software.

Live Cell Imaging

C6 cells were seeded in the confocal dish and then incubated for 24 hrs at 37 °C temperature under 5% CO₂. Probe **1** (5.0 μM) was then added into the cells with 30 min incubation period and after that camptothecin (100 μM) was added into cells. Then the cells were lively monitored for next 24 hrs at AIR Nikon Laser Confocal Microscope using bench top incubator maintained at 5% CO₂ and 37 °C temperature. Fluorescent images were captured at different time intervals: 0, 30, 60, 90, 120, 150, 180, 210, 240, 270 and 300 min *via*

live cell video capture at $\lambda_{\text{ex}} = 488$ nm after adding probe 1 and $\lambda_{\text{em}} = 500$ -550 nm.

Acknowledgements

M. K. & V. B. acknowledge the financial support from UGC (F. No. 42-282/2013(SR)), DST, & CSIR, New Delhi. N.G., S.I.R and M.G. acknowledges UPE/UGC/CSIR program for JRF/SRF/JRF. UGC, grants under University with Potential for Excellence (UPE) and Centre for Potential Excellence under Particular Area (CPEPA) schemes are acknowledged for providing infrastructural facilities to carry out the research work.

Notes and references

- 1 H. P. Kao, J. R. Abney and A. S. Verkman, *J. Cell Biol.*, 1993, **20**, 175–184.
- 2 (a) P. K. Luby, *Int. Rev. Cytol.*, 2000, **192**, 189; (b) M. J. Stutts, C. M. Canessa, J. C. Olsen, M. Hamrick, J. A. Cohn, B. C. Rossier and R. C. Boucher, *Science*, 1995, **268**, 847; (c) W. H. Reinhardt, *Biorheology*, 2001, **38**, 203.
- 3 (a) P. K. Luby, *Int. Rev. Cytol.*, 2000, **192**, 189; (b) S. Hortelano, M. L. G. Martin, S. Cerdan, A. Casteillo, A. M. Alvarrez, L. Bosca, *Cell Death and Differ.*, 2001, **8**, 1022; (c) L. M. Rebelo, J. S. De Sousa, J. M. Filho and M. Radmacher, *Nanotechnology*, 2013, **24**, 1.
- 4 (a) Z. Yang, Y. He, J. H. Lee, N. Park, M. Suh, W. Chae, J. Cao, X. Peng, H. Jung, C. Kang, and J. S. Kim, *J. Am. Chem. Soc.*, 2013, **135**, 9181; (b) Z. Yang, Y. He, J. H. Lee, W. S. Chae, W. X. Ren, J. H. Lee, C. Kang and J. S. Kim, *Chem. Commun.*, 2014, **50**, 11672; (c) I. L-Duarte, T. T. Vu, M. A. Izquierdo, J. A. Bull and M. K. Kuimova, *Chem. Commun.*, 2014, **50**, 5282; (d) M. A. Haidekker, T. P. Brady, D. Lichlyter and E. A. Theodorakis, *J. Am. Chem. Soc.*, 2006, **128**, 398; (e) Z. Yang, J. Cao, Y. He, J. H. Yang, T. Kim, X. Peng and J. S. Kim, *Chem. Soc. Rev.*, 2014, **43**, 4563; (f) T. Liu, X. Liu, D. R. Spring, X. Qian, J. Cui and Z. Xu, *Sci. Rep.*, 2014, **4**, 5418; (g) Y. Zhao, C. Y. Y. Yu, R. T. K. Kwok, Y. Chen, S. Chen, J. W. Y. Lam and B. Z. Tang, *J. Mater. Chem. B.*, 2015, **3**, 4993; (h) W. T. Yu, T. W. Wu, C. L. Huang, I. Chen and K. T. Tan, *Chem. Sci.*, 2016, **7**, 301-307; (i) H. P. Lai, R. C. Gao, C. L. Huang, I. C. Chen and K. T. Tan, *Chem. Commun.*, 2015, **51**, 16197-16200; (j) S. I. Reja, I. A. Khan, V. Bhalla, M. Kumar, *Chem. Commun.*, 2015, **52**, 1182-1185; (k) A. Vyšniauskas, M. Qurashi, N. Gallop, M. Balaz, H. L. Anderson and M. K. Kuimova, *Chem. Sci.*, 2015, **6**, 5773.
- 5 (a) N. Gupta, S. I. Reja, V. Bhalla, M. Gupta, G. Kaur and M. Kumar, *Chem. Commun.*, 2015, **51**, 10875; (b) H. Zhu, J. Fan, M. Li, J. Cao, J. Wang and X. Peng, *Chem. Eur. J.*, 2014, **20**, 4691; (c) X. Yin, Y. Li, Y. Zhu, X. Jing, Y. Li and D. Zhu, *Dalton Trans.*, 2010, **39**, 992.
- 6 (a) D. Ding, J. Liang, H. Shi, R. T. K. Kwok, M. Gao, G. Feng, Y. Yuan, B. Z. Tang and B. Liu, *J. Mater. Chem. B.*, 2014, **2**, 231.
- 7 F. Guo, W. P. Gai, Y. Hong, B. Z. Tang, J. Qin and Y. Tang, *Chem. Commun.*, 2015, **51**, 17257-17260.
- 8 (a) A. P. de Silva, T. S. Moody and G. D. Wright, *Analyst*, 2009, **134**, 2385; (b) N. Duvva, K. Sudhakar, D. Badgurjar, R. Chitta, L. Giribabu, *J. Photochem. Photobiol. A Chem.*, 2015, **312**, 8-19.
- 9 J. Shao, S. Ji, X. Li, J. Zhao, F. Zhou and H. Guo, *Eur. J. Org. Chem.*, 2011, **2011**, 6100.
- 10 D. C. Magri, J. F. Callan, A. P. de Silva, D. B. Fox, N. D. McClenaghan, and K. R. A. S. Sandanayake, *J. Fluoresc.*, 2005, **15**, 769.
- 11 M. G. Kurnikova, N. Balabai, D. H. Waldeck, and R. D. Coalson, *J. Am. Chem. Soc.*, 1998, **120**, 6121-6130.
- 12 (a) K. E. Knowles, E. A. McArthur and E. A. Weiss, *ACS Nano*, 2011, **5**, 2026; (b) S. Raut, J. Kimball, R. Fudala, H. Doan, B. Maliwal, N. Sabnis, A. Lacko, I. Gryczynski, S. V. Dzyuba and Z. Gryczynski, *Phys. Chem. Chem. Phys.*, 2014, **16**, 27037.
- 13 Gaussian 09, Revision A.02, M. J. Frisch, G. W. Trucks, H. B. Schlegel, G. E. Scuseria, M. A. Robb, J. R. Cheeseman, G. Scalmani, V. Barone, B. Mennucci, G. A. Petersson, H. Nakatsuji, M. Caricato, X. Li, H. P. Hratchian, A. F. Izmaylov, J. Bloino, G. Zheng, J. L. Sonnenberg, M. Hada, M. Ehara, K. Toyota, R. Fukuda, J. Hasegawa, M. Ishida, T. Nakajima, Y. Honda, O. Kitao, H. Nakai, T. Vreven, J. A. Montgomery, Jr., J. E. Peralta, F. Ogliaro, M. Bearpark, J. J. Heyd, E. Brothers, K. N. Kudin, V. N. Staroverov, R. Kobayashi, J. Normand, K. Raghavachari, A. Rendell, J. C. Burant, S. S. Iyengar, J. Tomasi, M. Cossi, N. Rega, J. M. Millam, M. Klene, J. E. Knox, J. B. Cross, V. Bakken, C. Adamo, J. Jaramillo, R. Gomperts, R. E. Stratmann, O. Yazyev, A. J. Austin, R. Cammi, C. Pomelli, J. W. Ochterski, R. L. Martin, K. Morokuma, V. G. Zakrzewski, G. A. Voth, P. Salvador, J. J. Dannenberg, S. Dapprich, A. D. Daniels, Farkas, J. B. Foresman, J. V. Ortiz, J. Cioslowski, D. J. Fox, Gaussian, Inc. Wallingford CT, 2009.
- 14 S. Zheng, P. L. M. Lynch, T. E. Rice, T. S. Moody, H. Q. N. Gunaratne and A. P. de Silva, *Photochem. Photobiol. Sci.*, 2012, **11**, 1675.
- 15 J. Cao, C. Hu, F. Liu, W. Sun, J. Fan, F. Song, S. Sun and X. Peng, *Chem. Phys. Chem.*, 2013, **14**, 1601.
- 16 M. V. Berridge, P. M. Herst and A. S. Tan, *Biotech. Ann. Rev.*, 2005, **11**, 127.
- 17 (a) A. Chiarugi and M. A. Moskowitz, *Science*, 2002, **297**, 259; (b) R. W. Johnstone, A. A. Ruefli and S. W. Lowe, *Cell*, 2002, **108**, 153; (c) S. W. Lowe and A. W. Lin, *Carcinogenesis*, 2000, **21**, 485.
- 18 A. N. Ketene, E. M. Schmelz, P. C. Roberts and M. Agah, *Nanomed. Nanotech. Biol. Med.*, 2012, **8**, 93.
- 19 L. M. Rebelo, J. S. De Sousa, J. M. Filho and M. Radmacher, *Nanotechnology*, 2013, **24**, 055102.
- 20 K. H. Dragnev, W. J. Petty and E. Dmitrovsky, *Cancer Biol. Therapy*, 2003, **2**, 150.
- 21 N. P. Mongan and L. J. Gudas, *Differentiation*, 2007, **75**, 853.
- 22 D. Wlodkowic, J. Skommer, and Z. Darzynkiewicz, *Methods Mol. Biol.*, 2009, **559**, 19-32.
- 23 H. Kataria, R. Wadhwa, S. C. Kaul and G. Kaur, *PLoS ONE.*, 2013, **8**, e55316.
- 24 (a) H. J. Halpern, G. V. R. Chandramouli, E. D. Barth, C. Yu, M. Peric, D. J. Grdina and B. A. Teicher, *Cancer Res.*, 1999, **59**, 5836; (b) K. Fushimi and A. S. Verkman, *J. Cell Biol.*, 1999, **112**, 719.
- 25 J. Włodarczyk and B. Kierdaszuk, *Biophys. J.*, 2003, **85**, 589.